Unravelling comorbidities contribution to cardiac diastolic dysfunction and heart failure

Authors: María Villalba-Orero[1,2,3], Marina López-Olañeta[1], Belén Campos-Olmo[1], Daniel Jimenez-Carretero[1], Lucía Sánchez[1], Fátima Sánchez-Cabo[1], Antonella Ausiello[1], Rodrigo Cañas-Álvaro[1], Emilio Camafeita[1], Jesús Vázquez[1,3], Pablo García-Pavía[1,3,6,7], Domingo Pascual-Figal[1,3,4,5], and Enrique Lara-Pezzi[1,3,*]

Affiliations: [1]Centro Nacional de Investigaciones Cardiovasculares (CNIC), Madrid, Spain. [2]Departamento de Medicina y Cirugía Animal, Facultad de Veterinaria, Universidad Complutense de Madrid, Spain. [3]Centro de Investigación Biomédica en Red Cardiovascular (CIBERCV), Madrid, Spain. [4]Biomedical Research Institute Virgen de la Arrixaca (IMIB-Arrixaca), Murcia, Spain. [5]Medicine Department, University of Murcia, Murcia, Spain. [6]Heart Failure and Inherited Cardiac Diseases Unit, Department of Cardiology, Hospital Universitario Puerta de Hierro Majadahonda, Madrid, Spain; [7]Universidad Francisco de Vitoria, Madrid, Spain.

*Correspondence: Dr. Enrique Lara-Pezzi, Myocardial Homeostasis and Cardiac Injury Programme, Centro Nacional de Investigaciones Cardiovasculares (CNIC), Melchor Fernandez Almagro, 3, 28029 Madrid, Spain. Tel.: +34-914531200, ext. 3309. email: elara@cnic.es

Total count: 6806 words

ABSTRACT

Background: Heart failure with preserved ejection fraction (HFpEF) is a major public health problem characterised by multiple simultaneous comorbidities whose specific contribution is challenging to disentangle in humans, leading to a generalized therapeutic approach that may not account for the underlying pathology. *Methods*: we followed distinct mouse models of major HFpEF comorbidities for 2.5 years to unveil their specific contribution to the syndrome. *Results*: All comorbidities contributed to HFpEF through partially distinct routes. Ageing alone resulted in HFpEF in old age, with delayed left ventricular relaxation and kidney fibrosis. Obesity induced a faster deterioration of relaxation associated with enlarged left ventricle and liver fibrosis. Hypertension caused delayed ventricular relaxation independent from structural changes that preceded left atrial dilatation linked to aortic stiffness, and increased fibrosis in myocardium and kidney. Chronic intermittent hypoxia led to HFpEF and relaxation impairment associated with pulmonary hypertension. Hyperglycaemia accelerated diastolic dysfunction and HFpEF onset associated with reduced arterial flow and left ventricular remodelling. Therefore, the pathological substrates contributing to HFpEF included cardiac and non-cardiac alterations with differential features for each comorbidity. Critically, the characteristics linked to diastolic dysfunction and HFpEF across the various comorbidities agreed with phenogroups observed in human patients. *Conclusions*: The identification of time-dependent pathological features provides a comprehensive picture of HFpEF progression associated with each comorbidity.

KEYWORDS: heart failure with preserved ejection fraction, ageing, obesity, hypertension, hyperglycaemia, sex-dependent effects, mouse models of heart failure.

INTRODUCTION

Heart failure is a major global health concern, particularly among the elderly, and is expecting to increase in the next years.[1] In stark contrast to heart failure (HF) with reduced ejection fraction (HFrEF), the prevalence of HF with preserved EF (HFpEF) is on the rise, and most large-scale clinical trials have proven ineffective in reducing mortality rates.[2] This lack of success can be partly attributed to marked patient heterogeneity, largely resulting from the large spectrum of non-cardiac comorbidities contributing to this complex syndrome.[3,4] HFpEF is closely linked to hypertension, obesity, diabetes mellitus, sleep apnea, and lung disorders, thereby complicating treatment strategies. Most patients accumulate several comorbidities at the time of presenting with symptoms of HF (stage C), and even at the time of detecting structural or functional abnormalities without HF (stage B). Therefore, it is challenging to discern the precise pathophysiological pathways underpinning the individual contribution of each comorbidity to the syndrome.

Recent clinical trials showed that SGLT2 inhibitors and GLP-1 analogues can mitigate HF hospitalisation and cardiovascular mortality in HFpEF.[5,6,7] While these findings are encouraging, the precise impact of age and the individual influence of comorbidities in driving diastolic dysfunction leading to HFpEF remains obscure. In order to develop new personalized approaches able to prevent cardiac dysfunction and HFpEF, it is essential to identify the specific features underlying the progression of cardiac dysfunction for each separated comorbidity.

Given the intricate interplay of various comorbidities in human patients and the interaction with aging, animal models represent an invaluable tool for unravelling the progression of diastolic dysfunction and HFpEF. However, suitable mouse models specifically simulating HFpEF are limited, challenging the translation from fundamental research to clinical application.[8] Indeed, animal models of HFpEF often show diastolic dysfunction but rarely demonstrate HF itself, a *sine qua non* condition to faithfully replicate human HFpEF, especially lung congestion.[8,9] Additionally, several animal models are based on genetic alterations or chemical inhibitors that induce HFpEF often at an unnaturally young age.[10,11] This is a critical point, considering that HFpEF primarily affects the elderly population.[1]

Therefore, we designed an experimental study that aimed to discern the specific contribution of individual comorbidities in the progression from cardiac dysfunction to

HFpEF, unravelling the intricate complexity of this multifaceted syndrome. We used long-standing mouse models of ageing, obesity, hypertension, sleep apnoea, and hyperglycaemia to simulate the natural course of the syndrome for each comorbidity, identifying the earliest structural and functional features of cardiac dysfunction and, finally, HFpEF.

METHODS

Detailed methods can be found in the supplementary material.

Data availability

The authors declare that all supporting data are available within the article and its online supplementary files.

Mice and study design

All experimental procedures were in accordance with institutional guidelines and approved by the Centro Nacional de Investigaciones Cardiovasculares' Institutional Animal Care and Research Advisory Committee and by the Regional Government of Madrid (PROEX 177/17, PROEX 191.5/22).

A total of 188 male and female C57BL/6 mice, starting at 10 weeks-old were used. Mice were randomly assigned to one of the following comorbidity groups using simple randomisation: Obesity (OB) induced by high-fat diet [45 kcal% (24 g%) palm oil-based fat, 35 kcal% (41 g%) carbohydrate, 20 kcal% (24 g%) protein]), systemic hypertension (SAH) induced by high-salt diet (HS, 8% NaCl), chronic intermittent hypoxia (CIH) induced by exposure to hypoxia (FiO_2 10%) during 8 hours in their light cycle, 5 days/week, or chronic hyperglycaemiav(HG) induced by injecting streptozotocin (STZ, 50mg/kg, 0.05mol/L) i.p for five consecutive days. An untreated group was included as a control (CTL group). Serial weight and arterial blood pressure measurement, blood collection, and cardiac, vascular, and pulmonary ultrasound were performed for up to 2.5 years until mice showed evidence of HFpEF, in which case they were euthanatized using a chamber gradually filled with CO_2, or died naturally. Mice showing signs of illness were humanely sacrificed. No data were excluded.

Noninvasive ultrasound assessment

Ultrasound was blindedly performed using a high-frequency ultrasound system with a 30-MHz linear probe. Two- dimensional (2D) and M-mode (MM) echography were performed at >230 frames/s, and pulse wave and tissue Doppler (PW and TDI, respectively) was acquired at 40 kHz. Mice were lightly anesthetized with 0.5–2% isoflurane in oxygen, administered via nose cone and adjusting the isoflurane delivery to maintain podal reflex.

RNA isolation, reverse transcription, and qRT-PCR.

Total RNA was extracted from LV, RV, lung, liver, and kidney samples from each mouse using TRIzol (Invitrogen). Reverse transcription was performed with 100 ng of total RNA using High-Capacity cDNA Archive Kit (Applied Biosystems). Quantitative reverse-transcribed PCR (qRT-PCR) was performed in 10 µl: 1 µl of cDNA, 5 µl Power SYBR® Green PCR Master Mix (Thermo Fischer Scientific) and 0.5 µl of 150 µM primer (Table S12).

RESULTS

Characterization of comorbidity models and time to HFpEF

We chose major comorbidities associated with HFpEF in humans: ageing (*CTL* group), obesity induced by a high-fat/high-carbohydrate diet (*OB* group), systemic arterial hypertension induced by a high-salt diet (*SAH* group), chronic intermittent hypoxia simulating sleep apnoea through daily 8-hour hypoxia exposure (*CIH* group), and chronic hyperglycaemia resulting from pancreatic β-cell ablation (*HG* group).

To discern the individual contribution of each comorbidity to HFpEF, echocardiography parameters were analysed every 4-8 weeks in all animals (Table S1). Treatment began at 8 weeks of age, and observations extended up to 2.5 years until mice developed signs of HFpEF or died naturally (Table S1). Mice were considered to have HFpEF when they showed evidence of lung congestion together with echocardiographic evidence of cardiac structural and/or functional abnormalities consistent with the presence of LV diastolic dysfunction/raised filling pressures.[12]

As shown in Fig. 1A-E, all groups developed the expected pathological changes associated with each comorbidity. Remarkably, all comorbidity groups developed HFpEF, including aged *CTL* mice. The presence of comorbidities accelerated the onset of HFpEF, especially in *SAH* and *HG* mice (Fig. 1F-H). No significant decline in ejection fraction was detected (Fig. 1E), except for a few remaining *SAH* mice at very old age.

Diverse diastolic dysfunction features across comorbidities

The development of features of cardiac diastolic dysfunction was monitored by echocardiography. We focused on parameters related to LV relaxation (IVRT, E and A mitral waves, and E/A ratio) and LV filling pressures (left atrium (LA) internal diameter and the ratio between E and E' waves), following established mouse echocardiography guidelines. As shown in Fig. 2A-F, all mouse groups presented features of diastolic dysfunction,[13,14] with changes arising in middle or advanced age, depending on the comorbidity (Fig. 2A-F).

To identify specific features of diastolic dysfunction in each comorbidity relative to others, a linear mixed-effects model was employed, incorporating natural cubic splines to address non-linear temporal alterations (Fig. 2G, Table S2). In addition, we investigated

whether changes in cardiac diastolic parameters correlated with ventricular remodelling and/or alterations in different vascular territories, including the aorta, pulmonary and carotid arteries (Fig. S1A-F, Fig. S2A-H, Table S1). Using a statistical model that facilitated the identification of lagged correlations, we discerned sequences of events (Fig. 3, Fig. S3-S7).

CTL mice showed a progressive deterioration of LV relaxation (reduced E/A ratio despite a relatively flat E wave curve), which correlated synchronously with LV remodelling (changes in LV mass and volume), indicating simultaneous development of LV remodelling and diastolic dysfunction with age. These changes preceded the increase in LV filling pressures (LA enlargement) at late stages, which correlated with increased stiffness and reduced flow in the aorta (Fig. 2A-G, 3, S3A, S3B).

OB mice showed larger LV volume and mass (Fig. S1A-G), suggesting LV volume overload leading to LV hypertrophy (LVH), as it happens in humans.[15,16,17] They developed a faster impairment of LV relaxation (significantly accelerated E wave velocity leading to a reduced E/A ratio), which correlated strongly with LV remodelling (larger mass and volume), but not with changes in vascular parameters, suggesting that LV remodelling is the main driver of diastolic function deterioration in these mice (Fig. 2A-G, 3, S4A, S4B).

SAH mice showed more severe relaxation defects than other comorbidities, indicated by significantly decreased E/A ratio and increased IVRT, together with higher LV filling pressures (larger LA dilatation) at late time points (Fig. 2A-G). Early relaxation defects (reduced E wave and E/A ratio) preceded changes in vascular stiffness (left common carotid artery pulsativity and resistivity indexes, LCCA PI and RI) and showed only mild correlation with myocardial remodelling parameters (Fig. 3, S5A, S5B). In contrast, the longer IVRT and higher LV filling pressures (LA diameter) correlated synchronously with increased vascular stiffness and LV mass. These results suggest that relaxation deterioration is independent from LV remodelling in this comorbidity, while higher LV filling pressure is strongly linked to vascular stiffness and myocardial hypertrophy.

CIH mice developed pulmonary hypertension (PH), as evidenced by the reduced pulmonary artery (PA) AT/ET ratio (Fig. 1C). They showed delayed LV relaxation impairment (decreased E/A ratio) compared to other groups and slightly lower LV filling pressures (LA diameter and E/E' ratio; note that E/E' has negative values). Relaxation

defects (reduced E/A ratio) showed delayed correlation with changes in PA flow and increased RV wall thickness (Fig. 3, S6A, S6B), suggesting a potential contribution of PH and RV hypertrophy to diastolic dysfunction in this model. This delayed correlation between changes in PA flow and diastolic dysfunction was unique to *CIH* mice.

Finally, *HG* mice developed acute relaxation deterioration (higher IVRT and a faster decrease in E/A) starting shortly after hyperglycemia onset and progressing faster than in other groups. However, LV filling pressures (LA diameter, E/E') were less affected compared to other comorbidities (Fig. 2A-G). Impaired relaxation (elevated IVRT) correlated strongly with reduced arterial stiffness and flow, and with LV wall thickness even if hearts were generally thinner in these mice (Fig. 3, S7A, S7B). These results suggest a strong vascular component in the development of diastolic dysfunction as a consequence of *HG*, in addition to LV remodelling.

In essence, while all mice developed diastolic dysfunction, diverse patterns emerged linked to each comorbidity. *CTL* mice developed relaxation complications with ageing mainly associated with LV remodelling. *OB* mice showed more profound relaxation deterioration resulting from larger LV remodelling than *CTL* mice. In *SAH* mice, relaxation impairment was independent from structural changes and preceded a second phase of more severe diastolic dysfunction that involved higher LV filling pressures associated with increased arterial stiffness and LV remodelling. *CIH* mice developed delayed LV relaxation impairment mainly associated to PH, changes in PA flow and RV remodelling. Finally, *HG* mice developed diastolic dysfunction much faster than any other model associated with poorer arterial flow and LV remodelling.

Determinants of the transition to HFpEF in each comorbidity

To identify the main structural and functional changes linked to an increased risk of HFpEF, a comprehensive univariate analysis was conducted using tailored survival models of time-to-HFpEF, while accounting for age and sex (Fig. 4A, Table S3). In addition, to further illustrate the different pathways to HFpEF, the analysis was narrowed down to the top 10 parameters with the lowest p-values in each comorbidity within the HFpEF risk model, contrasting final values across groups with *CTL* mice (Fig. 4B).

For *CTL* mice, HFpEF risk was associated mainly with increased arterial stiffness (LCCA RI, mean and peak pressure gradients) and also with most diastolic dysfunction parameters (Fig. 4A). Interestingly, reduced PA flow and RV hypertrophy also increased to HFpEF risk. This suggests that the arterial stiffening that accompanies ageing contributes to the development of HFpEF to a larger extent than other features like LV remodelling, which also increased the risk but to a lower extent (Fig. 4A).

In *OB* mice, increased HFpEF risk was mainly associated with changes in LV function and, to some extent, with LV structure (wall thickness and intraventricular dimensions), poorer LV relaxation (longer IVRT) and increased filling pressures (larger LA diameter). The contribution of changes in aortic and carotid flow to HFpEF risk was more modest than in other comorbidities (Fig. 4A, 4B).

For *SAH* mice, increased HFpEF risk was mainly associated with stiffer arteries and changes in arterial flow (LCCA PI and RI indexes, mean and peak pressure gradients, AbdAo PI and RI, PA AT and peak velocity). Additionally, the core markers of relaxation deterioration (prolonged IVRT, reduced E wave velocity, and E/A ratio) and to some extent a thicker LV wall intensified HFpEF risk (Fig. 4A, 4B).

CIH mice displayed a robust association between HFpEF risk and PH (diminished PA AT/ET). In addition, risk also increased with higher arterial stiffness (LCCA PI, AbdAo PI) and to a certain extent with LV remodelling parameters and markers of diastolic dysfunction (Fig. 4A, 4B).

Lastly, *HG* mice showed HFpEF risk significantly correlated with reduced arterial stiffness and flow, as well as with LV remodelling (smaller LV volume and thicker ventricular walls; Fig. 4A). Therefore, the main parameters associated with diastolic dysfunction in this model also increased HFpEF risk.

Collectively, these results underline the diverse routes leading to HFpEF, contingent upon the underlying comorbidity. Increased arterial stiffness was a major contributor to HFpEF in *SAH* and *CTL* mice, while the pathway to HFpEF was rather associated with LV remodelling in *OB* mice, with PH in *CIH* mice, and with reduced vascular flow and increased ventricular wall thickness in *HG* mice.

Molecular mechanisms underlying the contribution of each comorbidity to diastolic dysfunction

To delve into the molecular mechanisms underpinning the contribution of individual comorbidities to deteriorated LV relaxation, we initially conducted a comparison of protein expression and oxidation measured by MS proteomics in the LV of each experimental group at their respective latest time points, in relation to *CTL* mice (Fig. 5A, 5B, Tables S4-S8, Table S9). In *OB* mice, an elevated oxidative response was observed, accompanied by an increase in protein oxidation and proteins associated with the immune response. *SAH* hearts exhibited increased expression of sarcomeric components, alongside reduced levels of calcium handling proteins. As anticipated, cardiac tissue from *CIH* mice showed higher levels of hypoxia-related proteins, while *HG* mice displayed higher expression of proteins implicated in the response to oxidative stress and in mitochondrial activity, concomitant with an increase in protein oxidation (Fig. 5B).

Next, we explored the association between changes in molecular parameters, particularly those related to inflammation and fibrosis, and alterations of LV relaxation in each comorbidity. We quantified mRNA expression of various markers in the LV, RV, lung, liver, and kidney, in addition to genes encoding some of the differentially expressed proteins (Fig. 5C). We also quantified fibrosis by histology (Fig. 5D). These analyses were carried out at intermediate and final time intervals for each comorbidity (Fig. 5C-E, 6A-E). Given the accelerated development of HFpEF in *HG* mice, these time points were selected earlier and juxtaposed with age-matched mice from the *CTL* group.

CTL and *SAH* mice showed similar associations between reduced LV relaxation and myocardial fibrosis markers. In *CTL* mice, reduced LV relaxation (faster A wave, reduced E/A ratio, prolonged IVRT) exhibited a broad correlation with markers of LV, RV and kidney fibrosis and inflammation (Fig. 5E, 6A, 6E, Table S10). Similarly, in *SAH* mice, parameters associated with late relaxation impairment (prolonged IVRT) showed correlation with fibrosis and inflammation markers in the LV (Table S10; Fig. 5E). Notably, in *SAH* mice, kidney fibrosis was strongly linked to aortic stiffness and larger LV mass, implying an interconnected axis encompassing kidney fibrosis, aortic stiffness, LV hypertrophy, LV fibrosis, and late diastolic dysfunction, a pattern also evident to some degree in *CTL* mice (Table S10).

In contrast, *OB* mice showed low association of LV relaxation impairment with myocardial inflammation and fibrosis genes or with the clear increase in markers of the oxidative response (Sod1, Cat, Gstm1). Instead, parameters related to reduced relaxation (reduced E/A ratio, faster A and E waves) were associated with increased expression of inflammation or fibrosis markers in the liver (Fig. 5E, 6C, 6E, Table S10).

CIH mice displayed comparatively less LV inflammation and fibrosis than other groups (Fig. 5C, 5D). Impaired relaxation (reduced E/A ratio) showed no significant association with LV fibrosis, but correlated with some congestion-related genes in the lung (Fig. 6B, 6E, Table S10)..

HG mice showed an early increase in myocardial fibrosis (Fig. 5C, 5D). However, deteriorated LV relaxation (prolonged IVRT, reduced E/A ratio) correlated inversely with fibrosis as determined by qRT-PCR and histology (Fig. 5E, Table S10), suggesting that LV fibrosis is not a major mediator of diastolic dysfunction in this group. Similarly, despite the increase in mitochondrial mRNAs in *HG* mice (Fig. 5C), these markers correlated inversely with reduced LV relaxation parameters (Table S10). Instead, relaxation impairment (reduced E/A) was associated with increased expression of lung congestion markers (Aqp4, Aqp5, Spb; Table S10, Fig. 6E).

Sex-related differences in HFpEF development

Subsequent exploration into potential differences between female and male mice within each group shed light on interesting trends, although statistical significance varied (Fig. 7A-E). Female mice showed increased incidence of HFpEF in *CTL* and *SAH* mice and swifter progression at middle age, compared to their male counterparts (Fig. 7A, 7B). In both groups, female mice showed stronger association between time-to-HFpEF and reduced arterial flow than male mice (Fig. 7C). In addition, the association between LV relaxation deterioration (prolonged, IVRT, slower E wave velocity, reduced E/A ratio) and HFpEF risk was more prominent in female *SAH* mice. Renal fibrosis was also higher in female mice across all comorbidities (Fig. 7E). Together, these results suggest that the HFpEF phenotype associated with ageing and hypertension is primarily driven by female animals.

In contrast, HFpEF incidence was slightly higher in *OB* males. Male mice also showed greater expression of fibrosis-related genes in LV and liver, although this association was not confirmed by histology (Fig. 7A, 7E). The alignment of functional and structural

parameters with HFpEF risk remained parallel between sexes, despite differences within the top ten parameters at the final time point (Fig. 7C, 7D).

As in *CTL* and *SAH*, female *CIH* mice showed higher HFpEF incidence (Fig. 7A) and a stronger association of HFpEF risk with PH (reduced PA AT/ET ratio) and arterial stiffness (Fig. 7C, 7D). However, male mice experienced accelerated HF progression, coupled with higher gene expression of some lung fibrosis markers (Fig. 7B, 7E). These results suggest that different pathological processes may drive HFpEF progression in *CIH* mice, with a stronger vascular component in female mice. In *HG* mice, no prominent sex-based disparities emerged in HFpEF incidence, progression, or association with structural and functional parameters (Fig. 7C).

DISCUSSION

Our work investigated the distinct roles played by prominent HFpEF-associated comorbidities in the complex development of this syndrome. We unveiled the principal functional and structural factors that underlie HFpEF within each group, together with the pathophysiological mechanisms and phenotypic features associated with the diverse patterns of diastolic dysfunction.

Aligned with the human HF definition, our criteria for HFpEF in animals entailed the presence of tangible indications of lung congestion and evidence of cardiac structural and/or functional abnormalities consistent with the presence of LV diastolic dysfunction.[18,19] This approach effectively addressed a key limitation observed in various animal HFpEF models that show extensive LV diastolic dysfunction but frequently lack clinical HF symptoms.[20] Notably, aging emerged as a pivotal driver of HFpEF, mirroring the human scenario. Thus, our work underscores the critical need of employing aged animals to aptly model this human syndrome.

Phenotype-based patient grouping (Phenomapping) has emerged as a promising approach in human HFpEF patient classification, aiming to identify subgroups that could benefit from tailored treatments.[19,21,22] Regrettably, this systematic approach has not yet been extensively applied to animal HFpEF models, where a spectrum of phenotypes often leans towards severe diastolic dysfunction rather than true HFpEF manifestations.[20] Importantly, our models underscored distinct features associated with HFpEF, with primary determinants within each group that resemble different patient phenogroups.

Obesity induced faster LV relaxation deterioration associated with an early onset of LVH characterized by an evolving shift from concentric to eccentric hypertrophy as disease progressed. Relaxation impairment did not significantly correlate with myocardial fibrosis. Additionally, a slightly higher HFpEF incidence was observed in male mice. These findings are in agreement with the characteristics of the obese cardiometabolic patient phenogroup in humans, marked by elevated LV mass and E wave velocity, with a higher prevalence among males.[19]

Chronic systemic hypertension exacerbated LV relaxation decline induced by ageing and induced a more pronounced increase in LV filling pressures compared to *CTL* mice. In *SAH* mice, diastolic dysfunction was mainly linked to myocardial remodelling and aortic stiffness. Progression to HFpEF in this group was mainly dependent on increased arterial

stiffness. Although *CTL* mice developed HFpEF later, they showed similar traits and correlations to *SAH* counterparts. In both groups, impaired LV relaxation was associated with markers of myocardial and kidney fibrosis, while this correlation was less obvious in other comorbidities. Therefore, although LV fibrosis is a hallmark of the aged myocardium, it cannot be universally considered to be a cause of diastolic dysfunction and HFpEF, as this association may depend on the underlying pathological substrate. Both *SAH* and *CTL* groups showed a higher female prevalence, and their phenotypes were similar to that of the human aging-hypertensive phenogroup, which presents a slower E wave, fibrosis, hypertension, kidney disease, and a greater prevalence among female patients.[19]

CIH mice developed PH in the absence of other comorbidities, together with RV hypertrophy and RV systolic dysfunction – an indication of maladaptive right ventricular remodelling resulting from prolonged hypoxic exposure.[23] Abnormal LV relaxation in *CIH* mice was mainly associated with PH, which was a major contributor to increased HFpEF risk in this group. While not a direct match, the key traits of diastolic dysfunction and HFpEF within this group share some semblance with human phenogroups exhibiting pulmonary dysfunction – encompassing cases marked by dyspnoea or chronic obstructive pulmonary disease (COPD) – in which lower LV mass and RV involvement are observed.[19]

Finally, *HG* mice showed alterations in LV relaxation mainly associated with reduced vascular flow and LV remodelling, which also marked the transition to HFpEF in this group. Both diastolic dysfunction (including increase IVRT as we observed in our work) and vascular complications have been previously described in animal models and patients with type 1 diabetes,[24–26] and type 1 diabetes is strongly increased the incidence of heart failure in human patients.[27] Therefore, the identification of LV remodelling and alterations in vascular flow as drivers of HFpEF in this group fits with existing data in animals and patients.

Several limitations warrant consideration in our study. First, the diagnosis of heart failure was based solely on echography analysis (heart and lung), we did not use exercise capacity to determine the presence of HFpEF. We have not accounted for the potential cumulative impact of multiple comorbidities, a scenario frequently encountered in human cases. Our research was conducted using a single mouse strain; it remains plausible that different mouse strains could yield varying outcomes. Of note, three SAH, one OB and

one CIH mice showed a reduction of the LVEF at the very end of the study. Since previous LVEF measurements in each mouse were preserved, we decided to keep these mice in the HFpEF group. These mice would likely correspond to a HFpEF to HFrEF transition, as it occurs in some patients and especially among uncontrolled hypertensive individuals..

In summary, we unveil distinct trajectories leading to HFpEF in mice with diverse comorbidities (Fig. 8). To our knowledge, this is the first study to provide simultaneous longitudinal analysis of mouse phenogroups associated with HFpEF. The similarity between mouse and human phenogroups reinforces the notion that HFpEF is not a single pathological condition. While this remains a descriptive study, our findings imply that personalized therapeutic strategies aligned with individual underlying pathologies would enhance patient outcomes.

SOURCES OF FUNDING

Grants PID2021-124629OB-I00, TED2021-129774B-C22, PLEC2022-009235 from the Ministry of Science and Innovation (MCIN/ AEI/10.13039/501100011033), the European Union's NextGenerationEU/PRTR ("Plan de Recuperación, Transformación y Resiliencia de España") and Fondo Europeo de Desarrollo Regional (FEDER) to E.L-P, PEJ-2019-TL/BMD-12831 from Comunidad de Madrid to E.L-P and Juan de la Cierva Incorporación Grant (IJCI-2016-27698) to M.V-O. The CNIC is supported by the Instituto de Salud Carlos III (ISCIII), the Ministerio de Ciencia e Innovación (MCIN) and the Pro CNIC Foundation, and is a Severo Ochoa Center of Excellence (grant CEX2020-001041-S funded by MICIN/AEI/10.13039/501100011033).

DISCLOSURES

None. None of the authors have anything to disclose.

BIBLIOGRAPHY

1. Pfeffer MA, Shah AM, Borlaug BA. Heart Failure With Preserved Ejection Fraction In Perspective. *Circ Res* 2019;**124**:1598–1617.
2. Argulian E, Chandrashekhar Y, Shah SJ, Huttin O, Pitt B, Zannad F, Bonow RO, Narula J. Teasing Apart Heart Failure with Preserved Ejection Fraction Phenotypes with Echocardiographic Imaging: Potential Approach to Research and Clinical Practice. *Circ Res* 2018;**122**:23–25.
3. Gori M, Senni M, Gupta DK, Charytan DM, Kraigher-Krainer E, Pieske B *et al*. Association between renal function and cardiovascular structure and function in heart failure with preserved ejection fraction. *Eur Heart J* 2014:1–10.
4. González-López E, Gallego-Delgado M, Guzzo-Merello G, Haro-Del Moral FJ De, Cobo-Marcos M, Robles C, *et al*. Wild-type transthyretin amyloidosis as a cause of heart failure with preserved ejection fraction. *Eur Heart J* 2015;**36**:2585–2594.
5. Udelson JE, Stevenson LW. The Future of Heart Failure Diagnosis, Therapy, and Management. *Circulation* 2016;**133**:2671–2686.
6. Vaduganathan M, Docherty KF, Claggett BL, Jhund PS, Boer RA de, Hernandez AF *et al.* SGLT-2 inhibitors in patients with heart failure: a comprehensive meta-analysis of five randomised controlled trials. *Lancet* 2022;**400**:757–767.
7. Kosiborod MN, Abildstrøm SZ, Borlaug BA, Butler J, Rasmussen S, Davies *M et al*. Semaglutide in Patients with Heart Failure with Preserved Ejection Fraction and Obesity. *New Engl J Med.* 2023; 389:1069-1084.
8. Withaar C, Lam CSP, Schiattarella GG, Boer RA de, Meems LMG. Heart failure with preserved ejection fraction in humans and mice: embracing clinical complexity in mouse models. *Eur Heart J* 2021;**42**:4420–4430.
9. Ham WB van, Kessler EL, Oerlemans MIFJ, Handoko ML, Sluijter JPG, Veen TAB van *et al*. Clinical Phenotypes of Heart Failure With Preserved Ejection Fraction to Select Preclinical Animal Models. *JACC Basic Transl Sci* 2022;**7**:844–857.
10. Schiattarella GG, Altamirano F, Tong D, French KM, Villalobos E, Kim SY *et al.* Nitrosative stress drives heart failure with preserved ejection fraction. *Nature* 2019;**568**:351–356
11. Caravia XM, Fanjul V, Oliver E, Roiz-Valle D, Morán-Álvarez A, Desdín-Micó G *et al.* The microRNA-29/PGC1α regulatory axis is critical for metabolic control of cardiac function. *PLoS Biol* 2018;**16**:e2006247–e2006247.

12. McDonagh TA, Metra M, Adamo M, Baumbach A, Böhm M, Burri H, *et al*. 2021 ESC Guidelines for the diagnosis and treatment of acute and chronic heart failure. *Eur Heart J* 2021;42(36):3599-3726.
13. Villalba-Orero M, Garcia-Pavia P, Lara-Pezzi E. Non-invasive assessment of HFpEF in mouse models: current gaps and future directions. *BMC Med* 2022;**20**:349.
14. Schnelle M, Catibog N, Zhang M, Nabeebaccus AA, Anderson G, Richards DA, *et al*. Echocardiographic evaluation of diastolic function in mouse models of heart disease. *J Mol Cell Cardiol* 2018;**114**:20–28.
15. Russo C, Jin Z, Homma S, Rundek T, Elkind MSV, Sacco RL, Tullio MR Di. Effect of obesity and overweight on left ventricular diastolic function: a community-based study in an elderly cohort. *J Am Coll Cardiol* 2011;**57**:1368–1374.
16. Borlaug BA, Jensen MD, Kitzman DW, Lam CSP, Obokata M, Rider OJ. Obesity and heart failure with preserved ejection fraction: new insights and pathophysiological targets. *Cardiovasc Res* 2023;**118**:3434–3450.
17. Abel ED, Litwin SE, Sweeney G. Cardiac remodeling in obesity. *Physiol Rev* 2008;**88**:389–419.
18. Borlaug BA, Sharma K, Shah SJ, Ho JE. Heart Failure With Preserved Ejection Fraction: JACC Scientific Statement. *J Am Coll Cardiol* 2023;**81**:1810–1834.
19. Cohen JB, Schrauben SJ, Zhao L, Basso MD, Cvijic ME, Li Z, *et al*. Clinical Phenogroups in Heart Failure With Preserved Ejection Fraction: Detailed Phenotypes, Prognosis, and Response to Spironolactone. *JACC Heart Fail* 2020;**8**:172–184.
20. Ham WB van, Kessler EL, Oerlemans MIFJ, Handoko ML, Sluijter JPG, Veen TAB van *et al*. Clinical Phenotypes of Heart Failure With Preserved Ejection Fraction to Select Preclinical Animal Models. *JACC Basic Transl Sci* 2022;**7**:844–857.
21. Shah SJ, Katz DH, Selvaraj S, Burke MA, Yancy CW, Gheorghiade M *et al*. Phenomapping for novel classification of heart failure with preserved ejection fraction. *Circulation* 2015;**131**:269–279.
22. Woolley RJ, Ceelen D, Ouwerkerk W, Tromp J, Figarska SM, Anker SD *et al*. Machine learning based on biomarker profiles identifies distinct subgroups of heart failure with preserved ejection fraction. *Eur J Heart Fail* 2021;**23**:983–991.
23. Yeghiazarians Y, Jneid H, Tietjens JR, Redline S, Brown DL, El-Sherif N *et al*. Circulation Obstructive Sleep Apnea and Cardiovascular Disease A Scientific Statement From the American Heart Association. *Circulation* 2021;**144**:56–67.

24. Shigeta T, Aoyama M, Bando YK, Monji A, Mitsui T, Takatsu M *et al*. Dipeptidyl peptidase-4 modulates left ventricular dysfunction in chronic heart failure via angiogenesis-dependent and-independent actions. *Circulation* 2012;**126**:1838–1851.
25. Bjornstad P, Donaghue KC, Maahs DM. Macrovascular disease and risk factors in youth with type 1 diabetes: time to be more attentive to treatment? *Lancet Diabetes Endocrinol* 2018;**6**:809–820.
26. Suys BE, Katier N, Rooman RPA, Matthys D, Beeck LOL De, Caju MVL Du *et al*. Female Children and Adolescents With Type 1 Diabetes Have More Pronounced Early Echocardiographic Signs of Diabetic Cardiomyopathy. *Diabetes Care* 2004;**27**:1947–1953.
27. McAllister DA, Read SH, Kerssens J, Livingstone S, McGurnaghan S, Jhund P *et al*. Incidence of hospitalization for heart failure and case-fatality among 3.25 million people with and without diabetes mellitus. *Circulation* 2018;**138**:2774–2786.

FIGURES

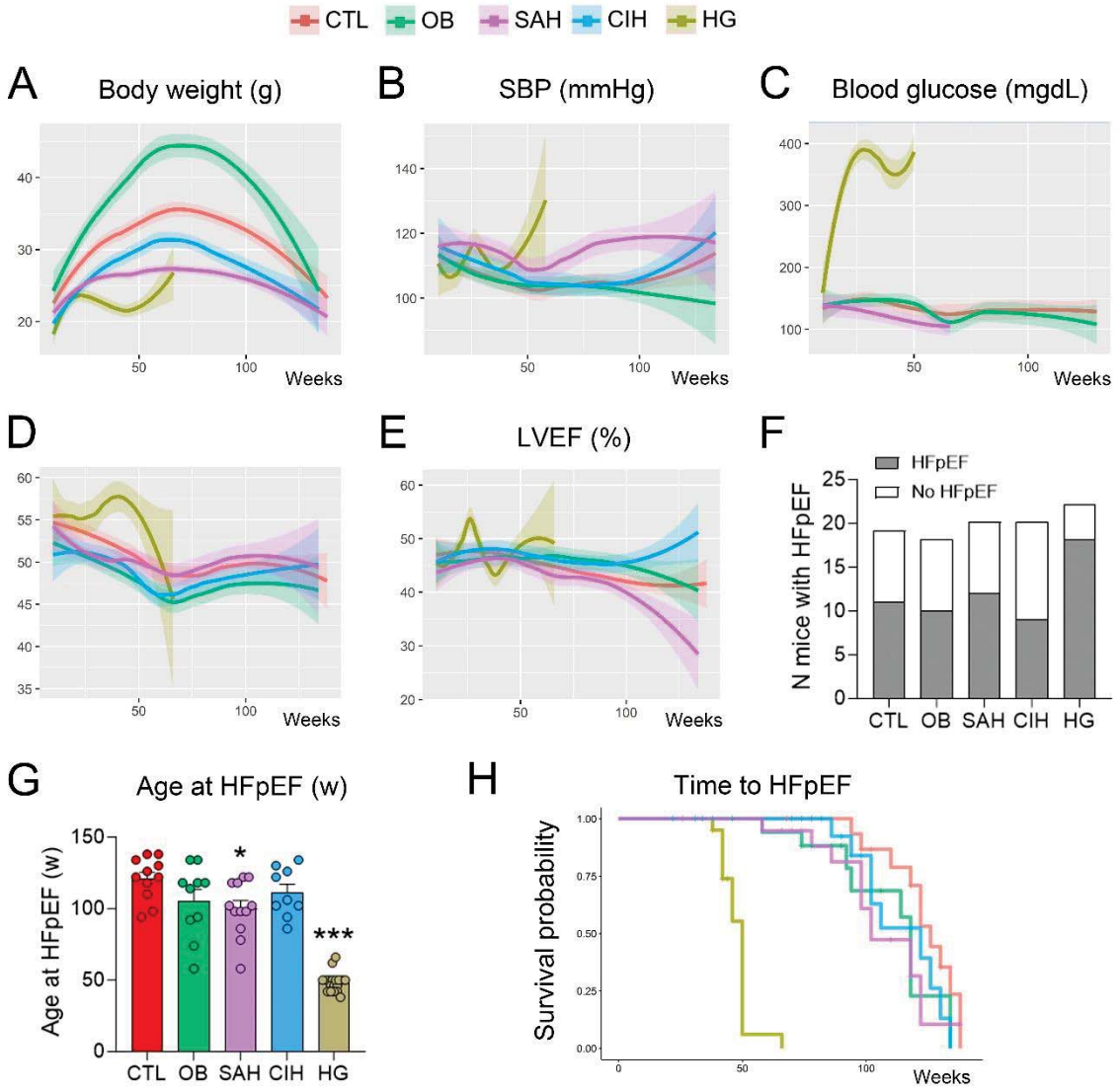

Figure 1. **All groups develop the expected pathological changes associated with each comorbidity.** (A-E) Body weight (A), systolic blood pressure (B), blood glucose (C), pulmonary artery acceleration time/ejection time ratio (D), and left ventricular ejection fraction (E) were measured every 2 months until mice developed HFpEF or died naturally. Lines and shadows represent means and their 95% CI, respectively, along time using smooth curves of values (loess). (F) Number of mice that developed HFpEF in each comorbidity. (G) Age at which mice developed HFpEF in each group. (H) Kaplan-Meier curve showing the probability of survival (no development of HFpEF) in the different groups. CTL, control; OB, obese; SAH, systemic arterial hypertension; CIH, chronic intermittent hypoxia; HG, hyperglycaemic.

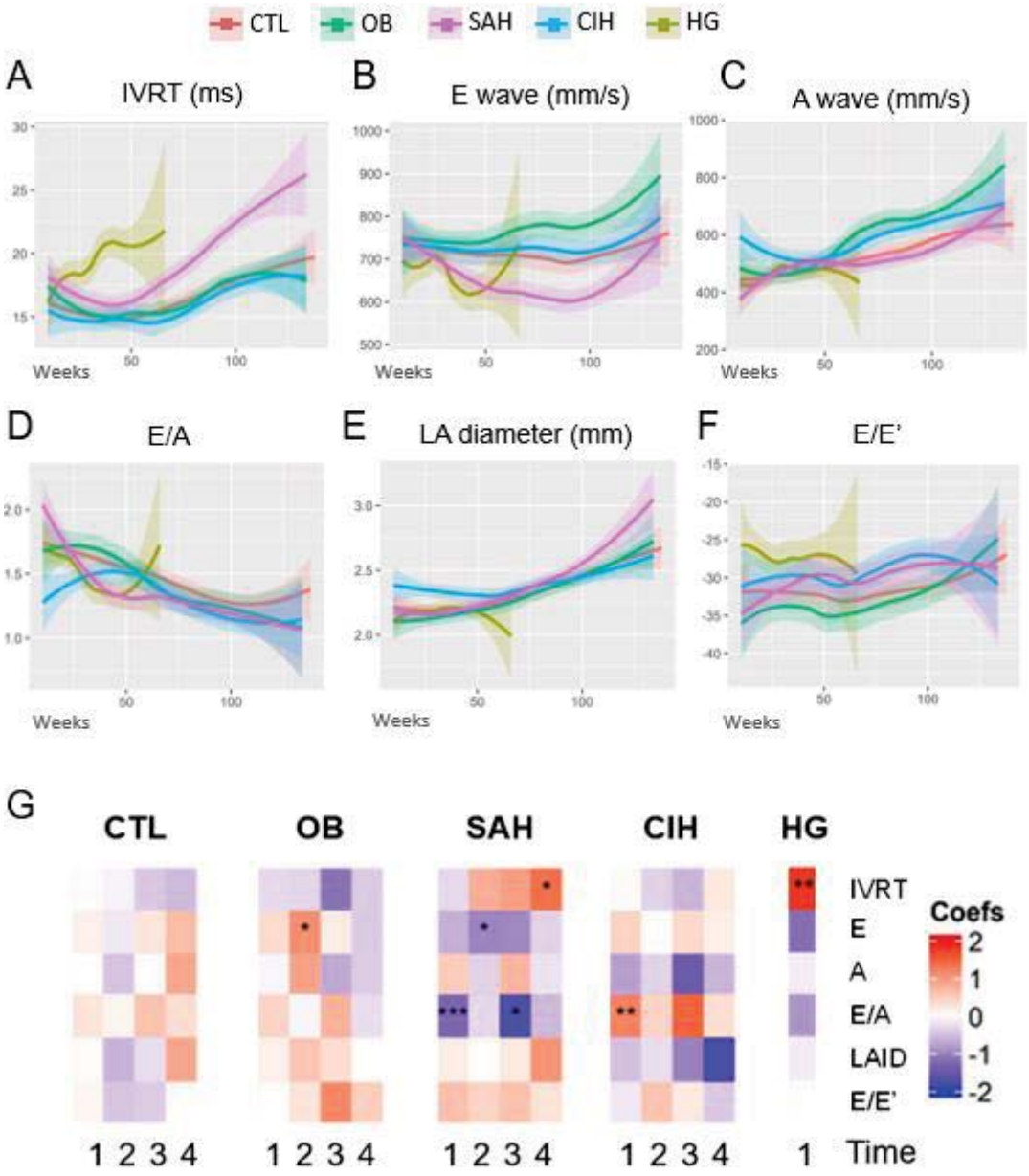

Figure 2. Distinct diastolic dysfunction patterns across comorbidities. (A-F), isovolumic relaxation time (IVRT; A), E and A wave velocities (B, C), the ratio between the velocity of the E and A waves (E/A; D), the ratio between the E and E' velocities (E/E'; E), and left atrium (LA) diameter (F) were measured by echocardiography every 2 months until mice developed HFpEF or died naturally. Lines and shadows represent means and their 95% CI, respectively, along time using smooth curves of values (loess). (G), To determine whether a specific parameter changed differently in a group compared to the rest of the groups, lmer was used to create a model that includes a fixed effect for group, a fixed effect for time (age), their interaction, and (uncorrelated) random intercepts and slopes for time, nested within each individual (adjusted for the impact of gender). Since the longitudinal variables do not change linearly in time, cubic splines were included natural to model the potential non-linearities. Each spline captures a different segment/interval of the relationship between 'age' and the outcome variable. Splines with 4 degrees of freedom were used, dividing the temporal effect in 4 time slots. The coefficient for a group represents the difference in the average response between the group and the rest of groups at time zero. *p<0.05, **p<0.01, ***p<0.001.

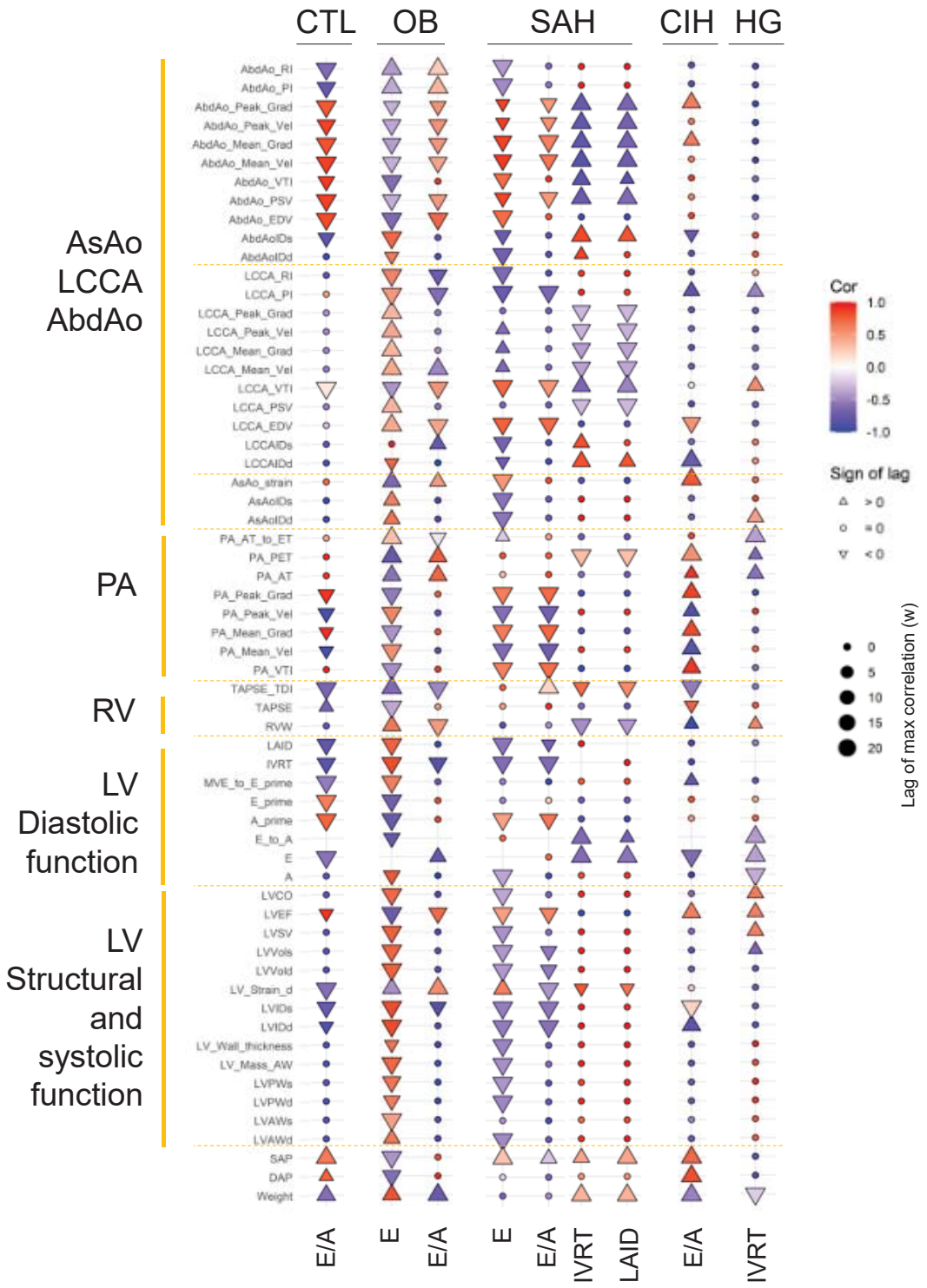

Figure 3. Diastolic dysfunction is associated with distinct cardiac and vascular parameters in each comorbidity group. The correlation of selected parameters related to LV relaxation deterioration (E, E/A, IVRT) and/or increased filling pressures (LAID) with different left ventricular (LV), right ventricular (RV), pulmonary artery (PA), ascending aorta (AsAo), left common carotid artery (LCCA), and abdominal aorta (AbdAo) functional and structural parameters was analysed taking into account potential time lags in the correlation. Triangle heading up means that the parameter in the Y axis

preceded the diastolic function parameter in the X axis; triangle heading down indicates that the parameter in the Y axis follows the diastolic function parameter in the X axis; circle means the correlation is synchronous. The size of the triangle indicates the degree of time lag. Red, direct correlation; blue, inverse correlation. Colour intensity corresponds with the R value. LV, left ventricle; LVAW and LVPW, LV anterior and posterior wall thickness, respectively; s, systole; d, diastole; ID, internal diameter; LVVol, LV volume, LVSV, LV stroke volume; LVEF, LV ejection fraction; LVCO, LV cardiac output; RVW, right ventricle wall thickness; PA, pulmonary artery; VTI, velocity time integral; Vel, blood flow velocity; Grad, pressure gradient; AT, acceleration time; ET, ejection time; AsAo, ascending aorta; LCCA, left common carotid artery; EDV, end diastolic volume; PSV, peak systolic velocity; PI, pulsativity index; RI, resistivity index; AbdAo, abdominal aorta. Statistical correlations of all parameters can be found in Fig. S3-S7.

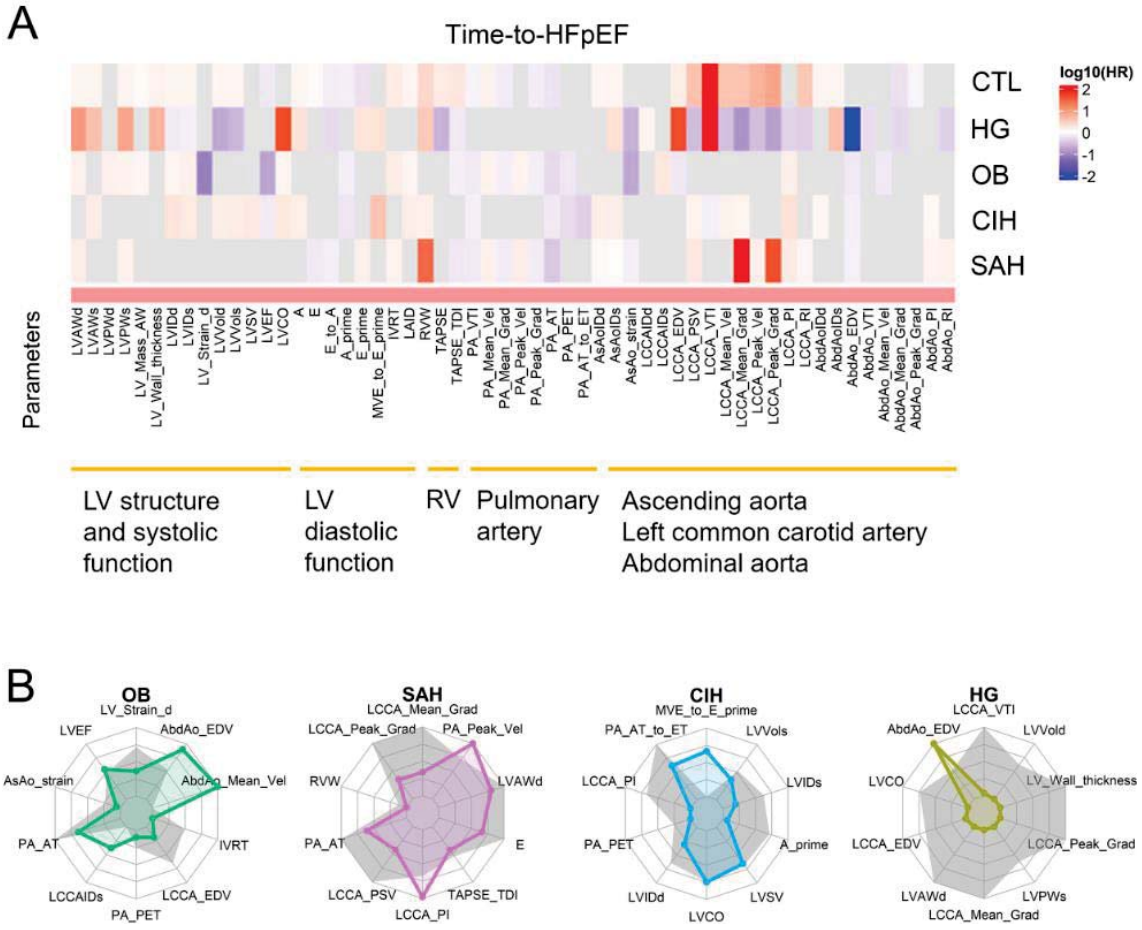

Figure 4. Distinct parameters are associated with the risk of HFpEF. (A) Analysis of time-to-HFpEF. Heatmap displaying variables with p-values of hazard ratios that are significant ($p<0.05$) for each comorbidity independently. Colour represents hazard ratios that indicate the change in the risk of HF event if the continuous parameter rises by one unit (one standard deviation in the case of standardized variables), displayed in log10 scale. Positive/negative HR values (red/blue) denote an increase/decrease, respectively. Grey denotes non availability or no significance. CTL, control; OB, obese; SAH, systemic arterial hypertension; CIH, chronic intermittent hypoxia; HG, hyperglycaemic. (B), Spider graphs showing main echocardiographic parameters associated with changes in the risk of HFpEF and their respective weight in each comorbidity. Grey represents values for the CTL group. Last available values were used to compute mean parameters per group. Mean values for each group are represented. For each individual parameter, inner/outer ring represents the minimum/maximum value among the 5 groups. Parameters are ordered based on Hazard Ratios (HR, decreasing order to prioritize the stronger effects), starting at the top and following a counterclockwise order.

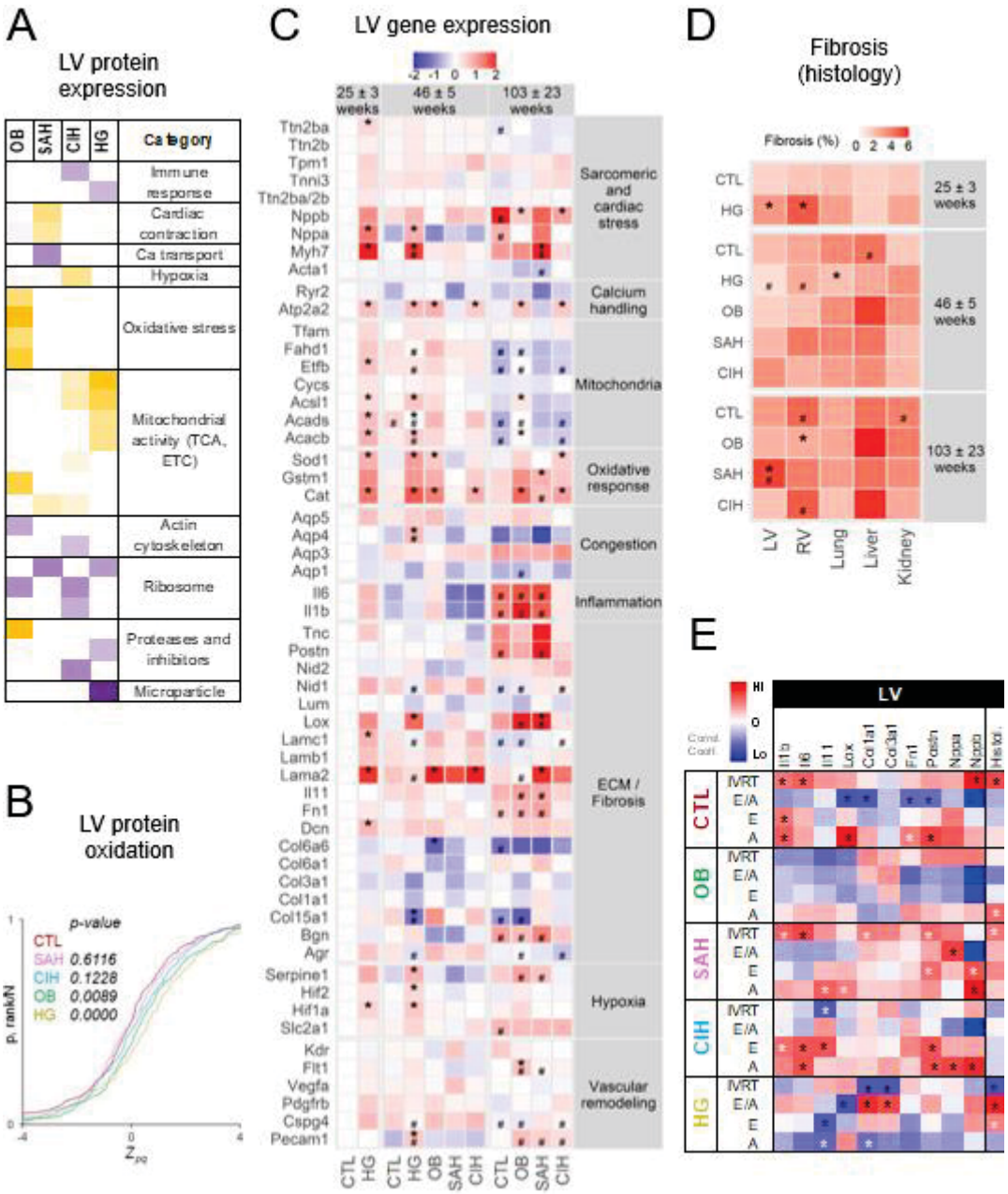

Figure 5. Relaxation impairment is associated with different pathophysiological changes in the left ventricle in each comorbidity. (A) Biological process categories enriched in proteins changed in each comorbidity compared to CTL in left ventricle analysed by mass spectrometry proteomics at their respective final time point (n=5 per group). (B) Cumulative distributions of the standardized log2 ratios of abundances (Zqp) of peptides containing oxidized cysteine residues. (C), Total mRNA was isolated from left ventricle and gene expression was analysed by qRT-PCR. Results show log2 fold-change for each gene in the different groups. Time points were divided into 25 ± 3 weeks (early time points); 46 ± 5 weeks (middle time points); and 103 ± 23 weeks (late time points reflecting the time when mice developed HFpEF or died naturally). Genes are

clustered according to biological process. For each gene, relative expression levels are shown with the highest as red and the lowest as blue. Significant differences (FDR-adjusted p-value<0.05) between each group and CTL mice at each time point are indicated by asterisk (*p<0.05, **p<0.01, ***p<0.001), and differences with the earliest time point within each group are indicated by the hash key ($^{\#}$p<0.05). n=7-19 male + female mice per group (see Table S1 for details). (D), Tissue fibrosis was analysed by picrosirius red staining in LV, RV and peripheral tissues. p<0.05 compared to CTL at each time point; $^{\#}$p<0.05 compared to the earliest time point in each group. n=7-20 (see Table S1). (E) Pearson correlation between LV diastolic function and LV expression of inflammation and fibrosis markers and natriuretic peptides. *p<0.05. Red, positive correlation; blue, negative correlation, with colour shades indicating the R value. Grey boxes highlight those parameters that changed significantly in each comorbidity (Figure 2). CTL, control; OB, obese; SAH, systemic arterial hypertension; CIH, chronic intermittent hypoxia; HG, hyperglycaemic. Histol., histological analysis of fibrosis.

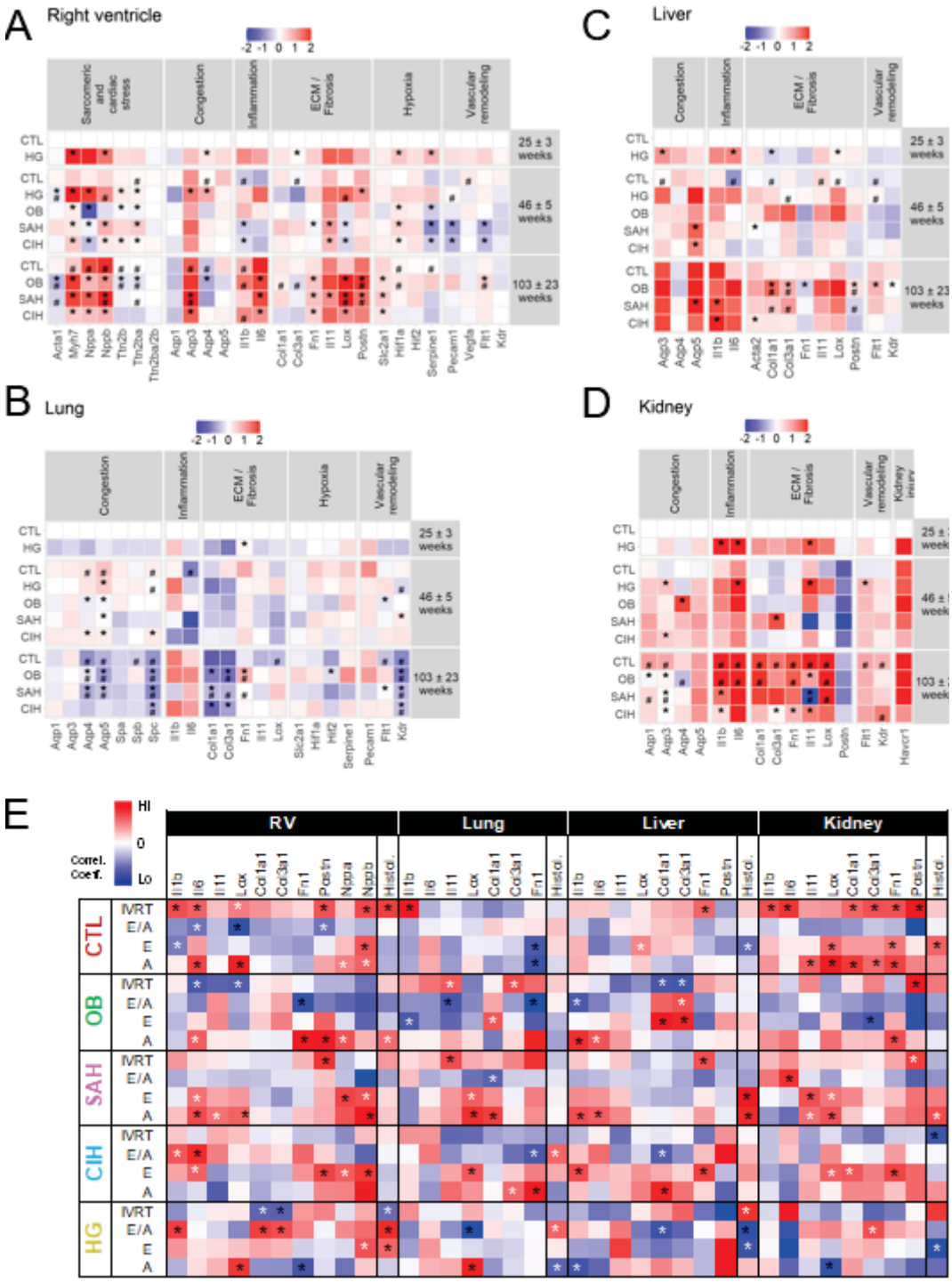

Figure 6. Left ventricular relaxation impairment is associated with pathophysiological changes in the right ventricle and peripheral organs. (A), Total mRNA was isolated from right ventricle, lung, liver and kidney, and gene expression was analysed by qRT-PCR. Results show log2 fold-change for each gene in each organ in the different groups. Time points were divided into 25 ± 3 weeks (early time points); 46 ± 5 weeks (middle time points); and 103 ± 23 weeks (late time points reflecting the time when mice developed HFpEF or died naturally). Genes are clustered according to biological process. For each gene, relative expression levels are shown with the highest as red and the lowest as blue. Significant differences (FDR-adjusted p-value<0.05) between each

group and CTL mice at each time point are indicated by asterisk (*p<0.05, **p<0.01, ***p<0.001), and differences with the earliest time point within each group are indicated by the hash key ($^{\#}$p<0.05). n=7-19 male + female mice per group (see Table S1 for details). (B), Pearson correlation between LV diastolic function and expression of inflammation and fibrosis markers and natriuretic peptides in the right ventricle, lung, liver, and kidney. *p<0.05. Red, positive correlation; blue, negative correlation, with colour shades indicating the R value. Grey boxes highlight those parameters that changed significantly in each comorbidity (Figure 2). CTL, control; OB, obese; SAH, systemic arterial hypertension; CIH, chronic intermittent hypoxia; HG, hyperglycaemic. Histol., histological analysis of fibrosis with picrosirius red.

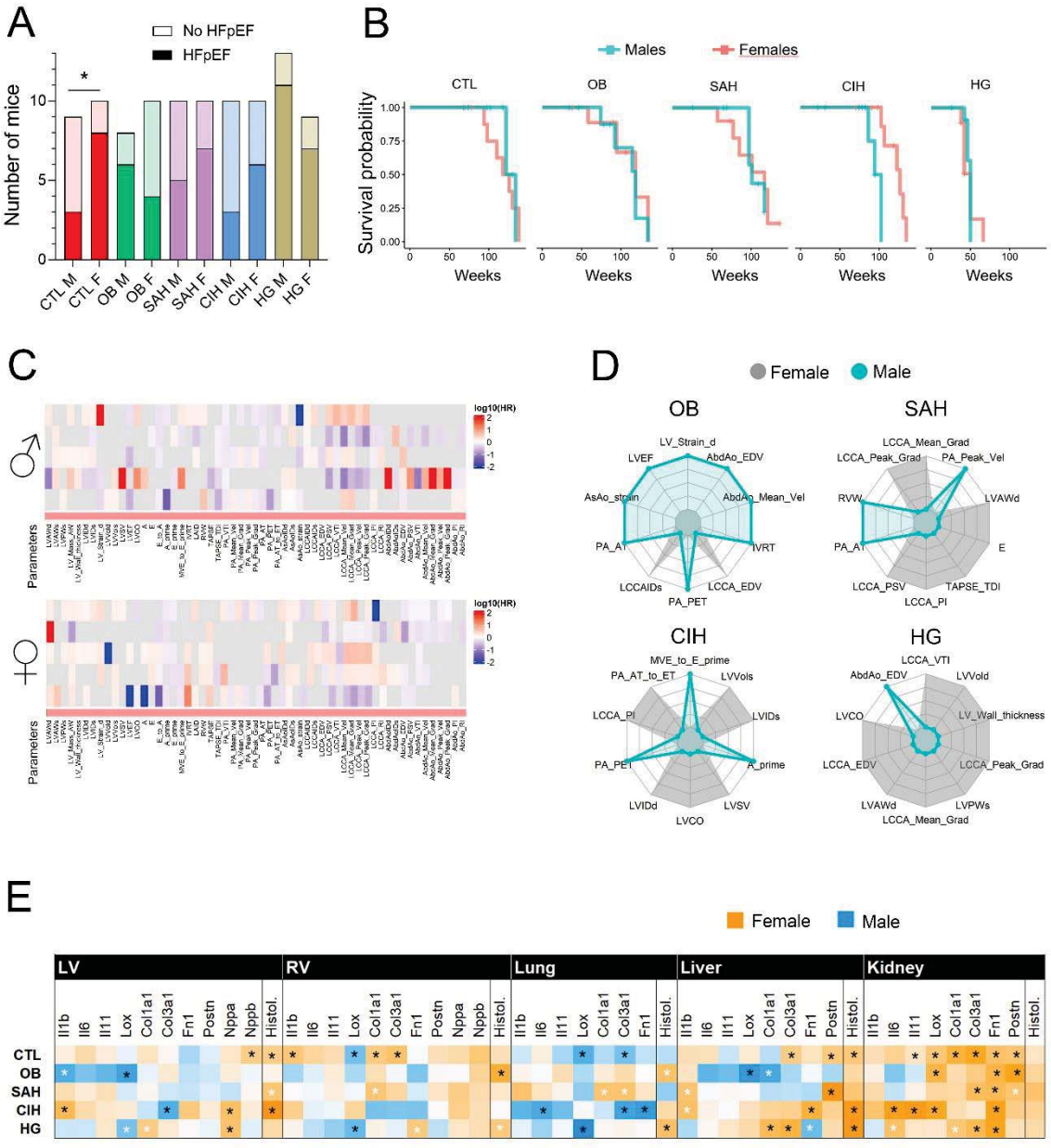

Figure 7. Sex-related differences in HFpEF development. (A) Incidence of HFpEF in male and female mice in each comorbidity. *p<0.05 male vs female, Fisher's test. (B), Kaplan-Meier curve showing the probability of survival (no development of HFpEF) in female and male mice, separately for each group. (C) Analysis of time-to-HFpEF in each comorbidity and sex. Heatmap displaying variables with p-values of hazard ratios that are significant (p<0.05) for each comorbidity independently. Colour represents hazard ratios that indicate the change in the risk of HFpEF event if the continuous parameter rises by one unit (one standard deviation in the case of standardized variables), displayed in log10 scale. Positive/negative HR values (red/blue) denote an increase/decrease, respectively. Grey denotes non availability or no significance. (D), Spider graphs showing main echocardiographic parameters associated with changes in the risk of HFpEF and their respective weight in each sex and comorbidity. Grey and blue represent values for female and male mice respectively. Last available values were used to compute mean parameters

per group. Mean values for each group are represented. For each individual parameter, inner/outer ring represents the minimum/maximum value among the 5 groups. Parameters are ordered based on Hazard Ratios (HR, decreasing order to prioritize the stronger effects), starting at the top and following a counterclockwise order. (E), Pearson correlation between sex and expression of inflammation and fibrosis markers and natriuretic peptides in the left ventricle, right ventricle, lung, liver, and kidney. *$p<0.05$. Blue, positive correlation with males; orange, positive correlation with females, with colour shades indicating the R value. CTL, control; OB, obese; SAH, systemic arterial hypertension; CIH, chronic intermittent hypoxia; HG, hyperglycaemic.

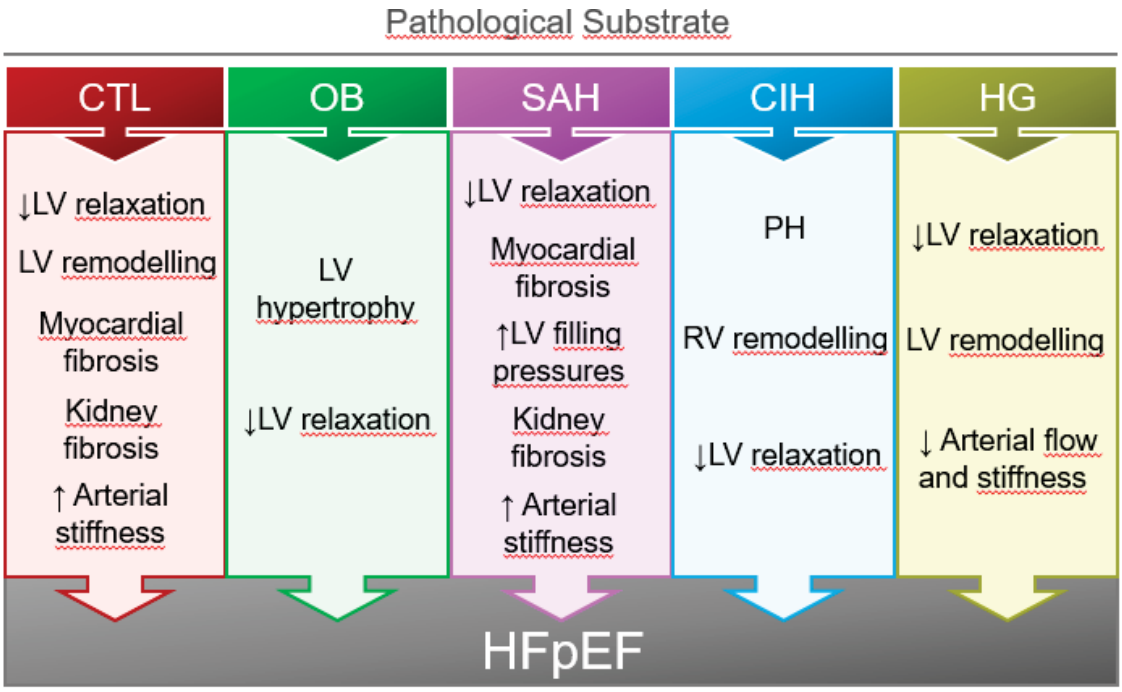

Figure 8. Schematic summarising the main routes to HFpEF depending on the underlying comorbidity.